cAMP-dependent phosphorylation of the tetrodotoxin-resistant voltage-dependent sodium channel SNS

E. M. Fitzgerald*†, K. Okuse*‡, J. N. Wood‡, A. C. Dolphin† and S. J. Moss†§

†*Department of Pharmacology*, ‡*Department of Biology and* §*MRC Laboratory of Molecular and Cell Biology, University College London, London WC1E 6BT, UK*

(Received 2 November 1998; accepted after revision 7 January 1999)

1. Protein kinase A (PKA) modulation of tetrodotoxin-resistant (TTX-r) voltage-gated sodium channels may underly the hyperalgesic responses of mammalian sensory neurones. We have therefore examined PKA phosphorylation of the cloned α-subunit of the rat sensory neurone-specific TTX-r channel SNS. Phosphorylation of SNS was compared with that of a mutant channel, SNS(SA), in which all five PKA consensus sites (RXXS) within the intracellular I–II loop had been eliminated by site-directed mutagenesis (serine to alanine).

2. *In vitro* PKA phosphorylation and tryptic peptide mapping of SNS and mutant SNS(SA) I–II loops expressed as glutathione-S-transferase (GST) fusion proteins confirmed that the five mutated serines were the major PKA substrates within the SNS I–II loop.

3. SNS and SNS(SA) channels were transiently expressed in COS-7 cells and their electrophysiological properties compared. In wild-type SNS channels, forskolin and 8-bromo cAMP produced effects consistent with PKA phosphorylation. Mutant SNS(SA) currents, however, were not significantly affected by either agent. Thus, elimination of the I–II loop PKA consensus sites caused a marked reduction in PKA modulation of wild-type channels.

4. Under control conditions, the voltage dependence of activation of SNS(SA) current was shifted to depolarized potentials compared with SNS. This was associated with a slowing of SNS(SA) current inactivation at hyperpolarized potentials and suggested a tonic PKA phosphorylation of wild-type channels under basal conditions.

5. We conclude that the major substrates involved in functional PKA modulation of the SNS channel are located within the intracellular I–II loop.

Mammalian sensory neurones express both tetrodotoxin-sensitive and tetrodotoxin-resistant (TTX-r) voltage-gated sodium channels. Recent work has led to the cloning from rat dorsal root ganglion neurones (DRGs), of the α-subunit of a TTX-r voltage-gated sodium channel, SNS (PN3) expressed in the small-diameter, C fibre neurones of the peripheral nervous system (Akopian *et al.* 1996; Sangameswaran *et al.* 1996). Functional expression of SNS in *Xenopus* oocytes has shown that the biophysical and pharmacological properties of this channel are similar to those described for endogenous TTX-r sodium channels found in small-diameter sensory neurones in culture (e.g. Roy & Narahashi, 1992; Ogata & Tatebayashi, 1993). Sensory neurone-specific TTX-r channels are associated predominantly with nociceptive neurones and it is therefore believed that they have an underlying role in nociceptive transmission (e.g. Arbuckle & Docherty, 1995; Villière & McLachlan, 1996). Importantly, the action of hyperalgesic agents such as serotonin and prostaglandin E_2 (PGE_2) on TTX-r channels in DRGs can be mimicked by drugs which upregulate cAMP-dependent protein kinase A (PKA) phosphorylation of the channels (England *et al.* 1996; Gold *et al.* 1996). PKA phosphorylation of TTX-r channels is therefore likely to be one mechanism underlying the hyperalgesic responses in sensory neurones. From this it follows that TTX-r channels are a potential target for therapeutic intervention in a range of pain states. In the present study we have therefore investigated PKA modulation of the cloned SNS channel.

Voltage-gated sodium channels are composed of a large α-subunit which contains all the structural elements necessary for function (Catterall, 1992). One or more β-subunits can modulate the voltage dependence and current kinetics of different channel isoforms (Isom *et al.* 1992, 1995*a*, *b*; Chen & Cannon, 1995; Qu *et al.* 1995) although it is not clear whether this is also the case for SNS.

* E. M. Fitzgerald and K. Okuse are joint first authors of this paper.

The α-subunit comprises four homologous domains, I–IV, each of which is composed of six membrane spanning segments, S1–S6. Within the intracellular linker region between IS6 and IIS1 (I–II loop) of the α-subunits of the rat brain IIA sodium channel there are five sites matching PKA consensus sequences as described by K/RXXS (X = any amino acid) (Kemp & Pearson, 1990), four of which have been shown biochemically to be involved in PKA phosphorylation of the channel (Murphy *et al.* 1993; Chen *et al.* 1995). Elimination of these PKA consensus sites by deletion and site-directed mutagenesis has shown that phosphorylation at Ser-573 is necessary and sufficient for PKA modulation of the channel currents, although phosphorylation at other positions (Ser-610 and Ser-623) also appears to be involved to a lesser extent (Smith & Goldin, 1996, 1997). Furthermore, PKC phosphorylation at Ser-1506 in the III–IV loop of this channel can enhance the level of PKA modulation observed (Li *et al.* 1993). PKA sites within the I–II loops of cardiac sodium channel α-subunits have also been shown biochemically and electrophysiologically to be sufficient for the functional effects of PKA phosphorylation in these channels, although the sites are distinct from those of the brain IIA channel (Murphy *et al.* 1996; Frohnwieser *et al.* 1997).

In common with the aforementioned sodium channels, five 'strong' PKA consensus sequences based on the motif RXXS, have been identified within the I–II loop of the SNS α-subunit (Fig. 1). We have used site-directed mutagenesis to remove these five consensus sites by substitution of alanine for serine residues in order to create a mutant SNS α-subunit, SNS(SA). By means of electrophysiological comparison of wild-type SNS with the mutant SNS(SA) channels, we have shown that removal of these five PKA consensus sites strongly reduces the degree to which SNS is modulated by cAMP-dependent phosphorylation. Thus, the major substrates necessary for PKA modulation of the SNS channel are located within the intracellular I–II loop.

METHODS

Materials

The following cDNAs were used: rat SNS (accession number X92184, Akopian *et al.* 1996), mutant rat SNS(SA) (Ser-463, Ser-487, Ser-499, Ser-510, Ser-536 point-mutated into alanine residues), and the mut-3 mutant of Green Fluorescent Protein (GFP) which was a gift from Dr T. Hughes (Yale University, New Haven, CT, USA).

Construction of SNS(SA) mutant

The rat SNS cDNA (Akopian *et al.* 1996) was cloned into the mammalian expression vector PGW-1 (*Hin*dIII–*Kpn*I sites). Site-directed mutagenesis was performed in this vector using uracil-containing vector as described in Yuckenberg *et al.* (1991), with the oligonucleotides 5′-TGACACCCTTGCTTTCACCCT-3′, 5′-CCT-AGGAAAGCCATCCTGCG-3′, 5′-ACTGCCGTGGTGCAGCCCC-TGCG-3′, 5′-GATGTCTTGGGGCGGGCGCTCG-3′ and 5′-CCAGC-AATATGGCACCTCGACGGC-3′ used to convert Ser-463, Ser-487, Ser-499, Ser-510 and Ser-536, respectively, into alanine residues. These mutations were confirmed by DNA sequence analysis. The mutated SNS cDNA, referred to as SNS(SA), was then subcloned as the *Hin*dIII–*Kpn*I fragment into the pMT2 expression vector (Genetics Institute, Cambridge, MA, USA) for transient expression in COS-7 (African green monkey kidney) cells (ECACC).

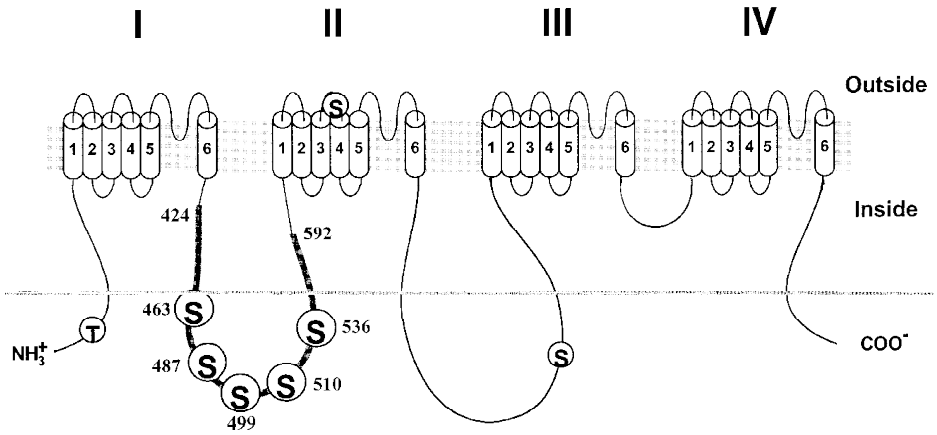

Figure 1. Schematic diagram of the α-subunit of SNS

The α-subunit of voltage-dependent sodium channels comprises four homologous domains, I–IV, each of which is composed of six membrane spanning segments, S1–S6. Within the intracellular linker region IS6 and IIS1 (I–II loop) of the SNS α-subunit there are five sites matching PKA consensus sequences at serine residues 463, 487, 499, 510 and 536. Site-directed mutagenesis was used to remove these PKA consensus sequences by substituting alanine residues for serines at these positions to create a mutant channel, SNS(SA). *In vitro* PKA phosphorylation was studied using GST fusion proteins of the I–II loop (residues Leu-424 to Gln-592; shown as thick line) of either wild-type GST-SNS or mutant GST-SNS(SA). An additional three putative PKA phosphorylation sites, two serines and a threonine, originally identified in the sequence of PN3 (Sangameswaran *et al.* 1996), are also present in the SNS sequence.

Expression and purification of glutathione-S-transferase fusion proteins

The wild-type SNS and mutant SNS(SA) channel intracellular I–II loop cDNAs (residues Leu-424 to Gln-592, see Fig. 1) were amplified using the polymerase chain reaction and cloned into p-GEX 2T (Smith & Johnson, 1988). The fidelity of the final expression constructs was verified by DNA sequencing. Glutathione-S-transferase (GST) fusion proteins were expressed in *E. coli* strain BL21. Purification was conducted as described previously by Moss *et al.* (1992).

Phosphorylation of fusion proteins by PKA

PKA phosphorylation of fusion proteins was carried out as described previously by Moss *et al.* (1992). Briefly, the fusion proteins (5 μg), either wild-type GST-SNS or mutant GST-SNS(SA), were phosphorylated in a volume of 100 μl of buffer (40 mM Hepes, pH 7·0, 20 mM $MgCl_2$, 0·4 mM ATP) for 15 min at 30 °C, using between 2 and 200 ng of the catalytic subunit of PKA purified from bovine heart (Promega). The reactions were terminated by the addition of EDTA to 25 mM, and separated by SDS PAGE followed by autoradiography. For determination of the stoichiometry of phosphorylation, reaction products were spotted onto 3 MM filters (Whatman) and washed in an excess of 10% trichloroacetic acid. Incorporation was then determined by scintillation counting.

Phosphopeptide mapping and phosphoamino acid analysis

Excised gel slices containing phosphoproteins were digested by trypsin and then subjected to 2-dimensional peptide mapping and autoradiography as described by Moss *et al.* (1992). Trypsin-digested peptides were also subjected to acid hydrolysis using 6 M HCl and the resulting phosphoamino acids were separated by thin-layer chromatography with phosphoamino acid standards, and subjected to autoradiography as described previously (Moss *et al.* 1992).

Transfection of COS-7 cells

COS-7 cells were grown to confluency in Dulbecco's modified Eagle's medium (DMEM) containing 10% newborn calf serum (Gibco/Life Technologies, Paisley, UK). Cells were transiently transfected with 20 μg of the appropriate cDNA construct plus 1 μg of mut-3 GFP-pMT2, by means of electroporation (Equibio Easyject electroporator, Flowgen, Lichfield, UK; 260 V, 1050 μF) in 500 μl of phosphate-buffered saline, pH 7·4. Successfully transfected cells were identified for electrophysiological recording by expression of GFP. Maximal GFP fluorescence and sodium channel expression were observed at 3–4 days post-transfection. The cells were harvested in a non-enzymic cell dissociation solution (Sigma) and replated directly onto 35 mm culture dishes in warmed DMEM. After replating, the cells were incubated at 27 °C until used for experiments.

Electrophysiology and solutions

Electrophysiological recordings were performed between 2 and 10 h after replating the cells as described above. Mean cell capacitance was approximately 20 pF. Cells were viewed briefly with a fluorescein filter block, and only small fluorescent cells expressing GFP, which were spatially isolated and had a compact morphology, were used in experiments. The whole-cell configuration of the patch-clamp technique (Hamill *et al.* 1981) was used to record sodium currents in the following solutions. The internal solution contained (mM): CsCl, 120; NaCl, 10; $MgCl_2$, 2·5; KCl, 5; Hepes, 5; EGTA, 5; K_2ATP, 0·5; adjusted to pH 7·2 with CsOH, adjusted to 290 mosmol l^{-1} with sucrose. The external solution contained (mM): NaCl, 100; $MgCl_2$, 2·5; KCl, 5; TEACl, 40; Hepes, 5; Na_2HPO_4, 2; $CaCl_2$, 0·01; glucose, 10; tetrodotoxin, 0·001; adjusted to pH 7·4 with NaOH, adjusted to 300 mosmol l^{-1} with sucrose. All experiments were performed at room temperature (20–22 °C). In some cells, a time-dependent increase in peak sodium current (I_{Na}) associated with a hyperpolarizing shift in the current–voltage relationship was observed during the initial period after establishing whole-cell mode. All the data presented here were therefore taken from currents which had been allowed to stabilize for up to 10 min before any measurements were made.

Patch pipettes of resistance 2–4 MΩ were pulled from thin-walled borosilicate glass tubing, fire-polished and coated with Sigmacote (Sigma). An Axopatch-1D amplifier (Axon Instruments) was used for recordings which were filtered at 2 kHz (4-pole Bessel filter) and digitized at 5–44 kHz using a Digidata 1200 A/D converter (Axon Instruments). The cells were held at a potential of −90 mV where the holding current was less than −0·05 nA and series resistance normally less than 10 MΩ. Currents were recorded with the cell capacitance compensated and leak currents subtracted using either a $P/4$ or $P/8$ subtraction protocol. Series resistance was compensated up to 80% and only cells which were adequately space clamped, as judged by a graded current activation, were used. Voltage errors from residual uncompensated series resistance and the liquid junction potential were less than 5 mV and no further correction was made. Data acquisition and analysis was performed using pCLAMP software (version 6.0.2, Axon Instruments) and Origin 3.5 (Microcal Software, Northampton, MA, USA).

Drugs or control solutions were perfused locally, from a distance of approximately 20 μm from the cell, by means of a computer-driven rapid drug application system (DAD 10; Adams & List, Westbury, NY, USA). Forskolin and 1,9-dideoxyforskolin were first dissolved in DMSO and then added to external solution to give a final concentration of 10 μM. The Na^+ salt of 8-bromo cAMP was dissolved directly in external solution and was used at a concentration of 100 μM. Veratridine, final concentration of 50 μM, was dissolved in ethanol before being added to the external medium. $CdCl_2$ (50 μM) was made up in external solution. All the reagents used were obtained from Sigma and stored as aliquots of stock solution at −20 °C, diluted, and used freshly each day.

The data are presented as means ± S.E.M. Statistical analysis was carried out by Student's t test, either paired or unpaired, as appropriate, using 95% confidence limits.

RESULTS

Phosphorylation of GST fusion proteins

Phosphorylation of the intracellular I–II loop of the SNS channel, expressed as a GST fusion protein (GST-SNS) was analysed *in vitro* using the catalytic subunit of PKA. The GST-SNS fusion protein exhibited a molecular mass of 48 kDa and could be purified to near homogeneity on immobilized glutathione. As well as a major band of 48 kDa, minor bands of approximately 38 kDa, which probably represent degradation products also co-purified. GST-SNS was rapidly phosphorylated by PKA *in vitro* using a low concentration of PKA (20 ng per assay; see Methods), to a final stoichiometry of 0·95 mol phosphate (mol protein)$^{-1}$ (Fig. 2*A*). The stoichiometry of phosphorylation observed could not be increased by incubation with higher concentrations of kinase up to 200 ng per assay, or extended time periods. The GST backbone is not a PKA substrate (Moss *et al.* 1992). Fusion protein phosphorylation was further examined by phosphoamino acid analysis in

combination with 2-dimensional tryptic peptide mapping. GST-SNS was phosphorylated predominantly on serine residues with trace levels of phosphothreonine also being observed (Fig. 2*B*). Tryptic peptide mapping resulted in the generation of nine reproducible phosphopeptides suggesting that GST-SNS is phosphorylated on multiple serine residues by PKA *in vitro* (Fig. 3*A*). Multiple phosphopeptides are produced since trypsin cleaves at the carboxyl side of Lys and Arg residues, and cleavage may occur at one or more of these positions to generate multiple peptides.

To examine whether these five residues are responsible for PKA phosphorylation of GST-SNS, site-directed mutagenesis was utilized. Based on the consensus motif of RXXS for PKA phosphorylation sites, serines 463 (RVKS), 487 (RRMS), 499 (RRAS), 510 (RAPS) and 536 (RRGS) within the SNS channel I–II loop were mutated to alanine residues in tandem (Kunkel, 1985). The phosphorylation of the resulting purified fusion protein, GST-SNS(SA), was then compared with that of the wild-type GST-SNS fusion protein using 20 ng PKA per assay. Mutation of these serine residues markedly reduced the stoichiometry of phosphorylation of the SNS intracellular I–II loop by PKA to 0·18 moles of phosphate per mole of protein (Fig. 2*C*). Phosphorylation of GST-SNS(SA) was also examined by phosphoamino acid analysis and peptide mapping. In common with the wild-type fusion protein, phosphorylation occurred predominantly on serine residues (Fig. 2*B*). In contrast, however, eight of the nine phosphopeptides produced on phosphorylation of the wild-type protein were eliminated on mutation of these serine residues (Fig. 3*B*). This residual phosphorylation of the mutant probably

Table 1. Biophysical properties of SNS and SNS(SA)

	SNS	SNS(SA)
I_{max} (pA pF^{-1})	−24·43 ± 6·52 (15)	−22·13 ± 5·19 (15)
V_{peak} (mV)	12·9 ± 1·6 (15)	20·0 ± 1·8 (15)*
V_{rev} (mV)	61·6 ± 1·3 (15)	63·2 ± 0·8 (15)
$V_{½}$ (mV)	−2·1 ± 1·4 (15)	8·8 ± 1·5 (15)***
k (mV)	8·5 ± 0·6 (15)	9·8 ± 0·6 (15)
τ_{act} at +15 mV (ms)	0·95 ± 0·13 (17)	0·94 ± 0·14 (15)
τ_{inact} at +15 mV (ms)	12·08 ± 0·77 (21)	16·90 ± 1·8 (20)*

I_{max} is the maximum peak current density and V_{peak} is the voltage at which the current density is maximal. Individual current density–voltage plots were fitted with a Boltzmann function:

$$I = (g(V - V_{rev}))/(1 + \exp(1 - (V - V_{½})/k)),$$

where V_{rev} is the sodium current reversal potential, $V_{½}$ is the voltage for half-maximal activation, k is the slope factor and g is conductance. Voltage dependence of activation data derived from individual current–voltage relationships were fitted with a Boltzmann function of the form:

$$G_{Na}/G_{max} = 1/(1 + \exp((V_{½} - V)/k),$$

where G_{max} is the maximum conductance. The peak conductance, G_{Na} at each test potential was calculated from the corresponding peak current, I_{Na} ($G_{Na} = I_{Na}/(V - V_{rev})$). The time constants of current activation and inactivation at peak current amplitude, τ_{act} and τ_{inact}, respectively, were determined by fitting single exponentials to the rising (τ_{act}) and decaying (τ_{inact}) phases of individual current traces, typically elicited by pulses of 200 ms. Statistically significant differences, determined using Student's t test, are denoted as follows: * $P < 0·05$, *** $P < 0·001$. The number of cells are given in parentheses.

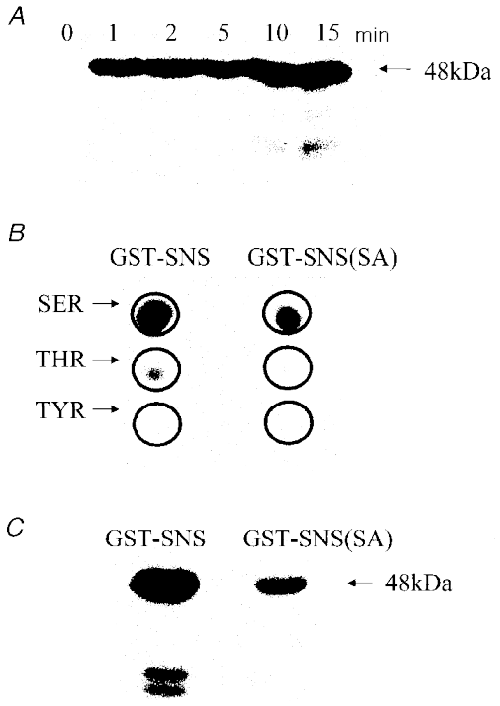

Figure 2. Phosphorylation of the wild-type GST-SNS and mutant GST-SNS(SA) fusion proteins by PKA

A, analysis of wild-type GST-SNS fusion protein phosphorylation by PKA. GST-SNS (5 μg) was phosphorylated *in vitro* by PKA (20 ng (100 μl buffer)$^{-1}$) for varying time periods (min) as shown. The extent of phosphorylation was then assessed by SDS-PAGE followed by autoradiography. GST-SNS was rapidly phosphorylated to a final stoichiometry of 0·95 moles of phosphate per mole of protein. *B*, phosphoamino acid analysis of wild-type GST-SNS and mutant GST-SNS(SA) fusion proteins. PKA-phosphorylated proteins were digested with trypsin followed by acid hydrolysis. The resulting phosphopeptides were then separated by TLC and visualized by autoradiography. The migration of standard phosphoamino acids is indicated. Wild-type GST-SNS is phosphorylated primarily on serine residues with trace levels of phosphothreonine. Mutant GST-SNS(SA) is phosphorylated to a lesser extent on serine residues. *C*, PKA phosphorylation of GST-SNS and mutant GST-SNS(SA) was compared. The extent of phophorylation was examined as in *A*. Mutation of the five serine residues markedly reduced the stoichiometry of phosphorylation to 0·18 moles of phosphate per mole of protein.

reflects phosphorylation of the non-PKA consensus threonine or serine residues within the GST protein fragment.

Together these *in vitro* phosphorylation studies support the view that serines 463, 487, 499, 510 and 536 are the major PKA substrates within the I–II loop of SNS, although it is possible that not all of these sites are equivalently phosphorylated *in vivo*.

Expression of SNS in COS-7 cells

Transient transfection of COS-7 cells with SNS cDNA resulted in a robust inward current, I_{Na}, with an average maximum current density, I_{max}, of $-24{\cdot}43 \pm 6{\cdot}52$ pA pF^{-1} at +15 mV ($n = 15$; Table 1). Inward current was observed in approximately 25% of GFP-expressing cells and no currents were observed in either non-transfected or mock-transfected cells (Fig. 4*A*).

Although no endogenous Na^+ currents were seen in non-transfected COS-7 cells, in order to confirm that the current elicited in SNS-transfected cells was attributable to SNS expression, further characterization was carried out. Akopian *et al.* (1996) previously showed in *Xenopus* oocytes that the sensitivity of the SNS current to divalent cations was similar to that reported for the DRG TTX-r current, 50 μM Pb^{2+} causing a greater inhibition than 100 μM Cd^{2+}. In DRGs, 50 μM Cd^{2+} has been shown to be ineffective on TTX-r current whilst being sufficient to block endogenous Ca^{2+} currents completely (Tatebayashi & Ogata, 1992; Ogata & Tatebayashi, 1993). Similarly, we observed that external application of 50 μM Cd^{2+} ($CdCl_2$) to SNS current expressed in COS-7 cells was without effect in all five cells tested (Fig. 4*B*).

Another means to confirm the nature of SNS I_{Na} was by application of the alkaloid veratridine. This agent has several actions on Na^+ channels including the inhibition of inactivation, hyperpolarization of voltage dependence of activation, and reduction of single-channel conductance (Hille, 1992). This results in large and prolonged tail currents after the return to the holding potential. The presence of external veratridine (100 μM) exerted profound effects on the I_{Na} recorded in all five cells tested (Fig. 4*C*). During the depolarizing step, usually to +15 mV, veratridine slightly reduced the amplitude of inward current. Repolarization to −90 mV revealed a slowly decaying tail current of increased amplitude compared with controls.

Finally, substitution of external Na^+ with equimolar choline chloride showed that inward I_{Na} was abolished by total replacement of Na^+ in the external solution whilst at 50 mM $[Na^+]_o$ (50%), current amplitude was approximately halved, from −189·8 to −96·7 pA, and the reversal potential shifted by 15·2 mV in a hyperpolarizing direction, close to the shift predicted from the Nernst equation ($n = 1$; data not shown).

The voltage dependence of activation of current was derived from current–voltage plots as outlined in the legend to Table 1. This gave a mid-point for current activation, $V_{½}$, of

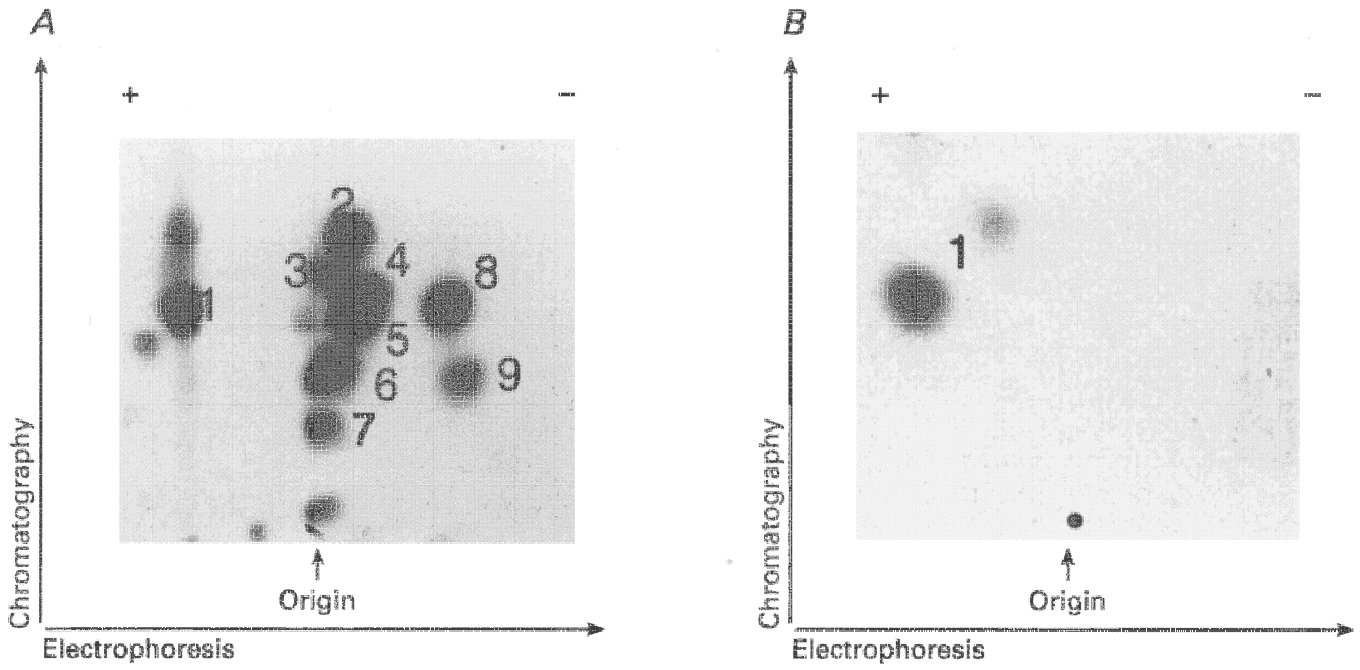

Figure 3. Tryptic peptide mapping of wild-type GST-SNS and mutant GST-SNS(SA)

Wild-type and mutant fusion proteins were phosphorylated as described in Fig. 2. Excised gel slices containing the respective phosphoproteins were digested with trypsin and subjected to 2-dimensional peptide mapping followed by autoradiography. PKA phosphorylation of GST-SNS generates 9 reproducible phosphopeptides, suggesting phosphorylation at multiple serine residues. Mutation of these five serines to alanine residues, however, resulted in 8 of the 9 phosphopeptides being eliminated.

$-2{\cdot}1 \pm 1{\cdot}4$ mV and a slope factor, k, of $8{\cdot}5 \pm 0{\cdot}6$ mV ($n = 15$; Fig. 5*A*). Representative current traces and the associated current–voltage plot from an SNS-transfected cell are illustrated in Fig. 5*B*. The voltage at which current density was maximal (V_{peak}) ranged from +5 to +25 mV, giving an average of $12{\cdot}9 \pm 1{\cdot}6$ mV ($n = 15$). This is consistent with the previously reported expression of SNS (PN3) in *Xenopus* oocytes where inward sodium currents typically peaked around +10 to +20 mV with 81–115 mM external Na^+ (Akopian *et al.* 1996; Sangameswaran *et al.* 1996). In common with SNS expression in *Xenopus* oocytes, therefore, the activation of I_{Na} observed in COS-7 cells was considerably more depolarized than the endogenous TTX-r sodium currents observed in DRGs, where V_{peak} is usually observed at between −10 and −20 mV. The reversal potential, V_{rev}, of $61{\cdot}6 \pm 1{\cdot}3$ mV ($n = 15$), however, was as expected based on the intra- and extracellular Na^+ concentrations (Table 1).

The rising phase of the current could be fitted with a single exponential, and the time constant of activation, τ_{act}, derived as a measure of activation rate. τ_{act} exhibited a clear voltage-dependent decrease as shown in Fig. 6*A*. Current decay could also be fitted by a single exponential, typically fitted to currents activated using 200 ms voltage steps. Figure 6*B* illustrates that the time constant of inactivation (τ_{inact}) also decreased steadily with depolarization. The decaying phase of the current at each voltage step was associated with a plateau phase which at peak current amplitude, typically around +15 mV, constituted $8{\cdot}9 \pm 1{\cdot}5\%$ ($n = 17$) of the current when measured as percentage current remaining at 100 ms. At the end of the 200 ms pulse, current was still not completely inactivated. The time constant for inactivation (τ_{inact}) at +15 mV averaged $12{\cdot}1 \pm 0{\cdot}8$ ms ($n = 21$), somewhat slower than might be expected for native TTX-r current (e.g. Elliott & Elliott, 1993; Ogata & Tatebayashi, 1993).

Together these data show that I_{Na} recorded in SNS-transfected COS-7 cells is a pure Na^+ current with properties qualitatively similar to the endogenous TTX-r current of DRGs.

Expression of mutant SNS(SA) in COS-7 cells

Transfection of SNS(SA) cDNA in COS-7 cells produced an inward I_{Na} in approximately 18% of GFP-positive cells. This current was similar to the wild-type SNS current (Table 1, Fig. 5*B*). The rising and decaying phases of the current could both be fitted by single exponential functions and the time constants for activation (τ_{act}) and inactivation

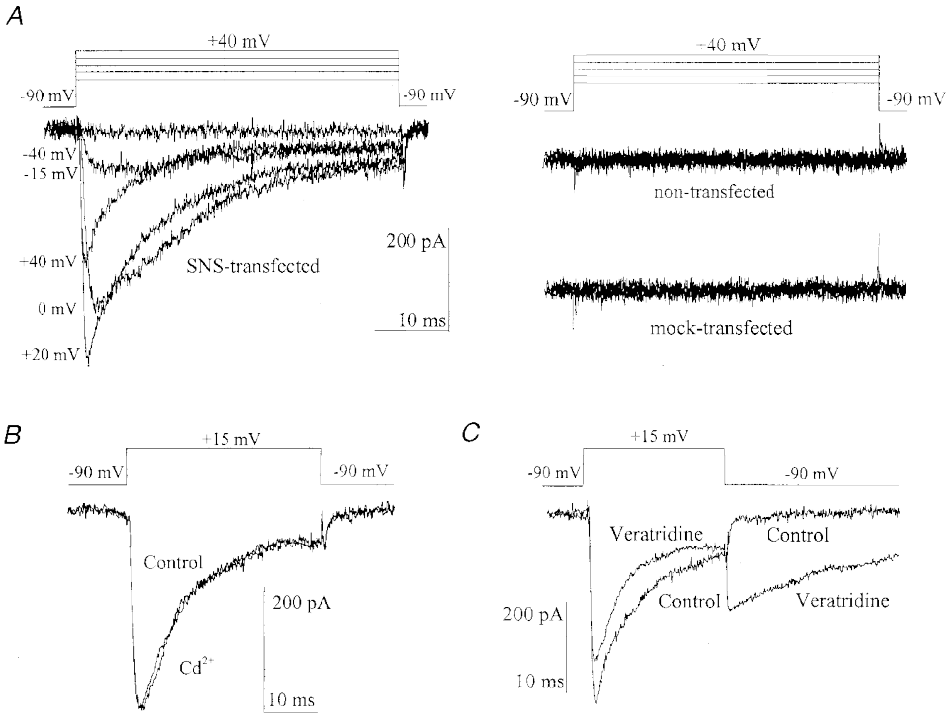

Figure 4. Characterization of SNS expressed in COS-7 cells

A, typical inward currents recorded in a COS-7 cell transiently transfected with SNS cDNA. These currents were evoked from a holding potential, V_h, of −90 mV by means of 40 ms depolarizing steps to −40, −15, 0, +20 and +40 mV. No inward currents were observed in either mock-transfected (expression vector only) or non-transfected cells using the same voltage protocol. *B*, representative traces showing the lack of effect of 50 μM Cd^{2+} on currents elicited at +15 mV from a V_h of −90 mV. *C*, typical traces illustrating the effects of 100 μM veratridine. During depolarizing steps to +15 mV, veratridine reduced the amplitude of inward current. Repolarization to −90 mV revealed a slowing decaying tail current of markedly increased amplitude compared with controls.

(τ_{inact}) again clearly decreased with depolarization (Fig. 6*A* and *B*). As with wild-type currents, the decaying phase of SNS(SA) at each voltage was associated with a plateau phase which at +15 mV constituted 9·1 ± 2·7 % ($n = 20$) of the peak current amplitude when measured at 100 ms. The maximum peak current density, I_{max}, was −22·1 ± 1·8 pA pF^{-1} ($n = 15$) and therefore not significantly different from the I_{max} observed for SNS current (Table 1). Importantly, however, the voltage dependence of activation (Fig. 5*A* and *B*) was significantly shifted by approximately 10 mV in a depolarizing direction ($V_{½} = 8·8 \pm 1·5$ mV, $n = 15$; $P < 0·001$) compared with wild-type SNS. I_{Na} peaked at between +10 and +30 mV, giving an average of 20·0 ± 1·8 mV ($n = 15$). No significant difference in either V_{rev} or k was observed between SNS and SNS(SA) (Table 1). Upregulation of cAMP-dependent phosphorylation has previously been reported to cause hyperpolarizing shifts in the current–voltage relationships of native TTX-r Na^+ channels (England *et al.* 1996). It is therefore possible that the depolarizing shift in activation of the mutant channel under control conditions may result from the removal of tonic PKA modulation normally associated with the wild-type channel.

There are also reports that PGE_2, which is believed to act via a cAMP–PKA pathway, can increase the TTX-r current activation and inactivation kinetics in adult DRGs (e.g. Gold *et al.* 1996). However, we found that whilst in some cells SNS(SA) current appeared to be more slowly activating than SNS currents, the averaged values of τ_{act} were not significantly slower (Fig. 6*A*). A significant slowing of τ_{inact}, however, was observed in SNS(SA) currents compared with SNS, at potentials between −10 and +15 mV (Fig. 6*B*). This was clearly shown when individual current traces elicited with short pulses were normalized to the peak and then averaged (see inset, Fig. 6*B*).

Effects of forskolin and 8-bromo cAMP on SNS and SNS(SA)

The effects of upregulating cAMP-dependent PKA phosphorylation in SNS- and SNS(SA)-transfected cells were monitored by comparing the properties of the currents before and after external application of either 10 μM forskolin or 100 μM 8-bromo cAMP. 1,9-Dideoxyforskolin (10 μM) was used as a control for non-PKA-related effects of forskolin. The data from these experiments are summarized in Table 2.

Figure 7*A–C* shows typical SNS currents evoked by repeated depolarizing steps within the range +5 to +20 mV, from a holding potential (V_h) of −90 mV. Application of forskolin, which directly activates adenylyl cyclase, produced a time-dependent increase in current amplitude from −209·1 ± 54·3 pA to −365·0 ± 85·6 pA ($n = 8$, $P < 0·001$; 82·7 ± 16·0 %). This effect was slowly reversible upon washing with control solution. In general, peak current

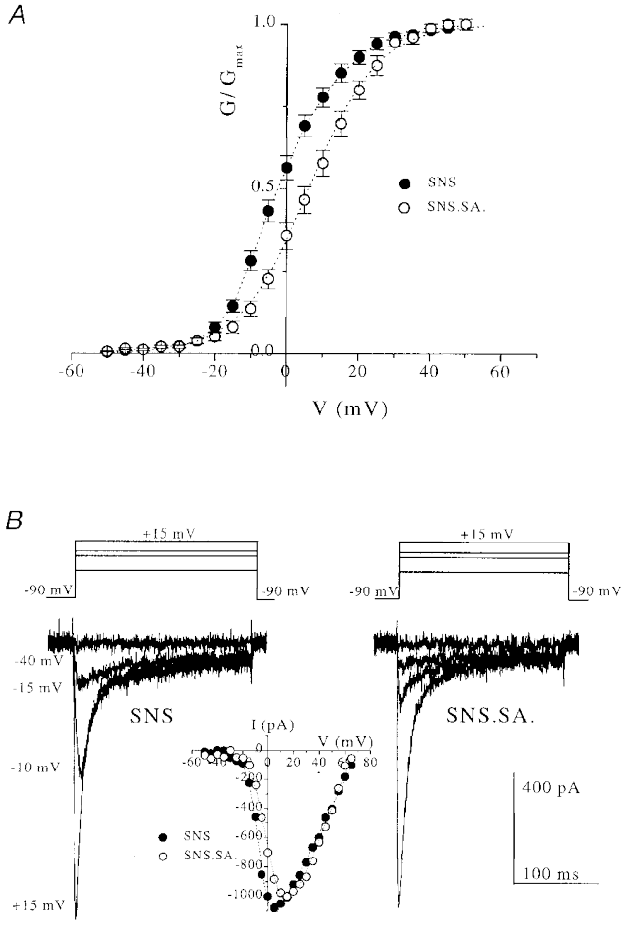

Figure 5. Comparison of voltage dependence of current activation in wild-type SNS and mutant SNS(SA) which lacks five PKA consensus sites within the intracellular I–II loop

A, conductance–voltage relationships were derived from individual current–voltage plots as described in the legend to Table 1. The derived values for voltage dependence of activation in SNS (●, $n = 15$) were $V_{½} = -2·1 \pm 1·4$ mV and $k = 8·5 \pm 0·6$ mV; and for SNS(SA) (○, $n = 15$), $V_{½} = 8·8 \pm 1·5$ mV, $k = 9·8 \pm 0·6$ mV. Currents were activated by depolarizing steps from −50 to +60 mV in 5 mV increments from a holding potential of −90 mV. *B*, representative currents and associated current–voltage plots from a wild-type SNS-transfected cell (●) and a cell transfected with mutant SNS(SA) (○). Currents were evoked using 200 ms depolarizing pulses to −40, −15, −10 and +15 mV from V_h of −90 mV. The current–voltage plots were fitted with a Boltzmann function to give the following values for SNS: $V_{½} = -11·5$ mV, $k = 5·0$ mV, $V_{rev} = 70·0$ mV; and for SNS(SA): $V_{½} = -5·1$ mV, $k = 6·9$ mV, $V_{rev} = 67·1$ mV.

Table 2. Effects of 10 μM dideoxyforskolin, 10 μM forskolin and 100 μM 8-bromo cAMP on the electrophysiological properties of SNS and SNS(SA)

Clone	Drug	τ_{act} at +15 mV (ms)	τ_{inact} at +15 mV (ms)	$V_{½}$ (mV)	k (mV)
SNS	Control	0·97 ± 0·14 (6)	12·19 ± 1·05 (7)	1·7 ± 3·5 (4)	8·0 ± 0·7 (4)
	Dideoxyforskolin	1·02 ± 0·14	11·33 ± 0·85	2·7 ± 4·3	9·3 ± 1·2
	Control	0·86 ± 0·10 (6)	12·77 ± 3·11 (5)	1·7 ± 6·00 (4)	7·7 ± 1·5 (4)
	Forskolin	1·36 ± 0·21	12·59 ± 3·11	−6·1 ± 5·4 *	6·7 ± 1·1
	Control	0·87 ± 0·09 (6)	9·09 ± 0·67 (5)	3·7 ± 3·7 (4)	7·8 ± 0·5 (4)
	8-Bromo cAMP	0·88 ± 0·09	9·09 ± 0·40	1·1 ± 5·5	9·5 ± 1·6
SNS(SA)	Control	0·95 ± 0·10 (5)	11·84 ± 1·90 (5)	11·1 ± 3·4 (3)	10·2 ± 0·3 (3)
	Dideoxyforskolin	0·92 ± 0·36	12·03 ± 3·30	7·1 ± 1·6	9·6 ± 1·1
	Control	0·96 ± 0·09 (6)	12·24 ± 1·13 (5)	5·9 ± 6·1 (3)	7·2 ± 0·7 (3)
	Forskolin	1·28 ± 0·40	12·46 ± 0·68	4·00 ± 5·8	7·3 ± 0·5
	Control	1·09 ± 0·17 (5)	11·53 ± 0·55 (5)	3·00 ± 3·7 (5)	9·2 ± 1·2 (5)
	8-Bromo cAMP	1·02 ± 0·21	11·41 ± 1·73	0·1 ± 3·1	7·9 ± 0·9

$V_{½}$, and k are as previously defined in the legend for Table 1. τ_{act} and τ_{inact} refer to the time constants of current activation and inactivation, respectively. * Statistically significant difference from control, as determined by Student's paired t test, $P < 0·05$. The number of cells per treatment is shown in parentheses.

amplitude started to return to control levels within 5–10 min of commencing control washes. There was also a marked hyperpolarizing shift in the current–voltage relationship from −7·8 ± 5·4 to −14·3 ± 6·1 mV ($n = 4$, $P < 0·05$). This effect may also be reversible. In one cell, forskolin caused a 15 mV hyperpolarizing shift of the current–voltage relationship followed by a depolarizing shift of 5 mV after washing with control solution for approximately 6 min. No effects were observed on the activation or inactivation kinetics. Dideoxyforskolin had no significant effect on current amplitude or the current kinetics, and failed to produce a shift in the voltage dependence of

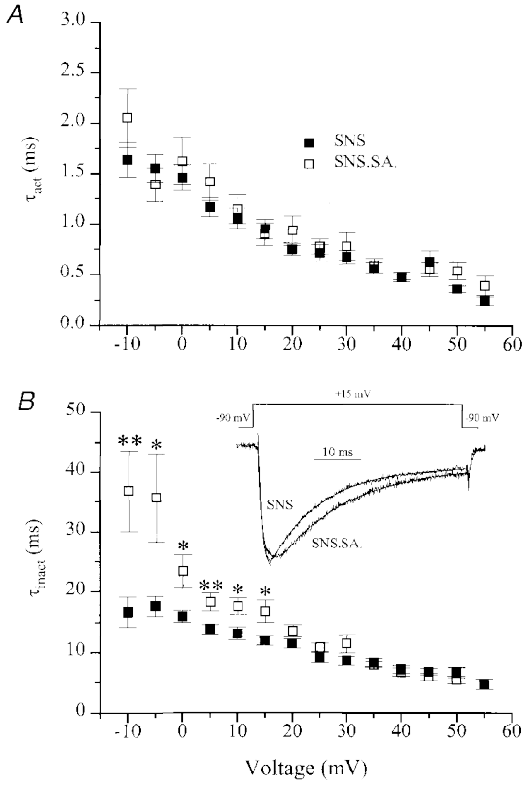

Figure 6. Current kinetics compared in SNS and SNS(SA)
A, the time constant of activation (τ_{act}) for SNS (■) and SNS(SA) (□). The rising phase of current at each voltage step was fitted with a single exponential and τ_{act} derived as a measure of activation rate. *B*, the time constant of inactivation (τ_{inact}) derived from single exponential fits to the decaying phase of current. Asterisks indicate statistically significant differences between SNS and SNS(SA): * $P < 0·05$ and ** $P < 0·01$ (Student's unpaired t test). The inset shows averaged currents for SNS- ($n = 14$) and SNS(SA)-transfected cells ($n = 12$). Individual currents were evoked by short 40 ms pulses to +15 mV and normalized to the peak amplitude prior to averaging. Continuous lines indicate single exponential fits of τ_{act} and τ_{inact} for SNS ($\tau_{act} = 0·86$ ms, $\tau_{inact} = 10·79$ ms) and SNS(SA) ($\tau_{act} = 0·69$ ms, $\tau_{inact} = 15·27$ ms).

activation. In the presence of dideoxyforskolin, I_{max} was $-302{\cdot}6 \pm 117{\cdot}8$ compared with $-307{\cdot}1 \pm 107{\cdot}0$ pA ($n = 7$). When 8-bromo cAMP was applied, again a time-dependent increase in current amplitude of $68{\cdot}1 \pm 14{\cdot}9\%$, from $-272{\cdot}6 \pm 90{\cdot}2$ to $-434{\cdot}3 \pm 149{\cdot}7$ pA ($n = 9$, $P < 0{\cdot}05$) was observed which was also slowly reversible. The time course for reversibility of these effects was similar to that previously described for forskolin. On average, a significant shift in the voltage dependence of activation was not found. However, in one cell of four, a hyperpolarization of 7 mV was observed following application of 8-bromo cAMP. No effects on either the kinetics of activation or inactivation were observed (Table 2). Thus, although 8-bromo cAMP does induce effects which are consistent with upregulation of the cAMP-PKA pathway, it appears relatively less efficient than forskolin. Whilst 8-bromo cAMP is widely used in both biochemical and electrophysiological studies of cAMP-dependent phosphorylation, it is not highly lipophilic and furthermore, is known to be hydrolysed by a variety of phosphodiesterases, thus reducing its efficiency in intact cells (Sandberg *et al.* 1991; MacFarland *et al.* 1991).

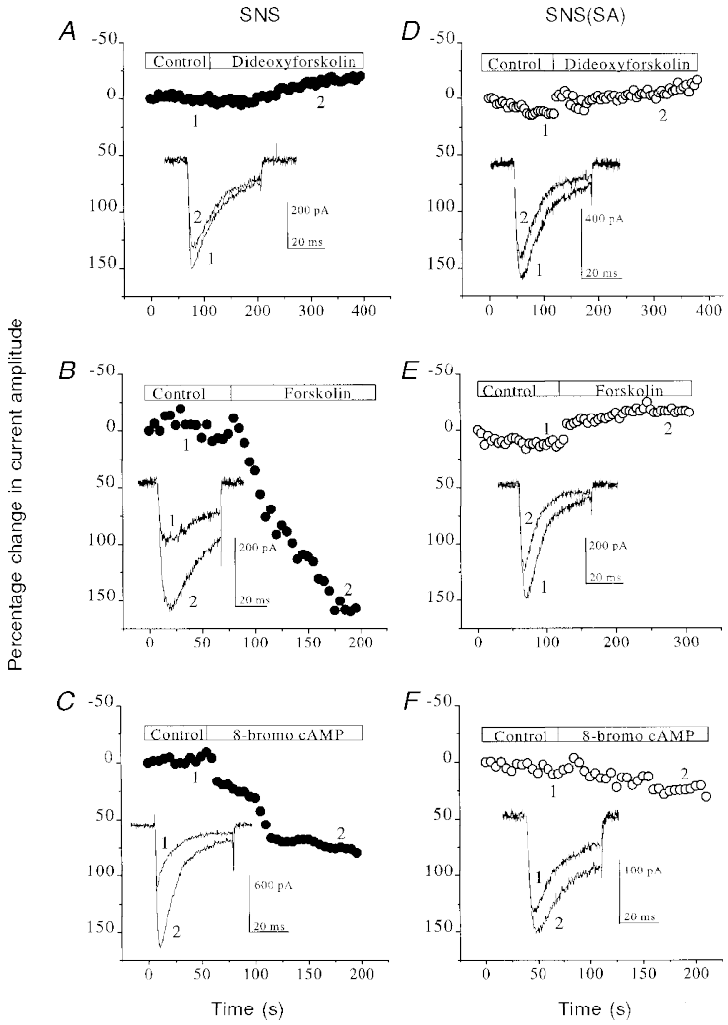

Figure 7. Effects of 10 μM dideoxyforskolin, 10 μM forskolin and 100 μM 8-bromo cAMP on SNS and SNS(SA)

Each panel (*A*–*F*) shows a representative time course, plotted as the percentage change in current amplitude relative to peak current amplitude at time $t = 0$ s (0%). The inset for each panel shows the associated current traces recorded at time points 1 and 2 as indicated on the plots. Scale bars refer to the absolute values of current amplitude in pA. *A*, lack of significant effect of dideoxyforskolin on SNS. *B*, example of SNS current steadily increasing in amplitude following application of forskolin. *C*, increase in SNS current amplitude observed in the presence of 8-bromo cAMP. *D*, dideoxyforskolin had no significant effect on SNS(SA) current. *E*, forskolin was ineffective on SNS(SA) currents as was 8-bromo cAMP, although in the example shown here (*F*) there was a slight increase in current amplitude. No effects on current kinetics were observed during any of the above treatments in either SNS or SNS(SA). In all cases, currents were activated from a V_h of -90 mV by stepping to depolarized potentials, typically +15 mV for SNS currents or +20 mV for SNS(SA) currents.

Figure 7*D–F* illustrates SNS(SA) currents evoked at between +10 and +30 mV from a V_h of −90 mV. As with SNS-transfected cells, dideoxyforskolin had no significant effect on current amplitude, I_{max} being $-283{\cdot}6 \pm 75{\cdot}6$ pA compared with $-252{\cdot}1 \pm 84{\cdot}5$ pA ($n = 6$) in control solution. Similarly, neither the voltage dependence of activation nor current kinetics were altered in the presence of this drug. In contrast to the situation for wild-type SNS, when forskolin was applied to SNS(SA)-expressing cells, no significant change in current amplitude was observed on average ($I_{max} = -272{\cdot}5 \pm 100{\cdot}6$ pA in controls and $-216{\cdot}9 \pm 63{\cdot}2$ pA in forskolin-containing solution, $n = 6$). Again, neither current kinetics nor voltage dependence of activation was affected (Table 2). This was also true in the presence of 8-bromo cAMP where I_{max} was $-551{\cdot}1 \pm 265{\cdot}9$ pA compared with $-516{\cdot}4 \pm 273{\cdot}6$ pA ($n = 7$) in control solution.

Comparison of the percentage changes in current amplitude between wild-type SNS and the mutant SNS(SA) following drug application is shown in Fig. 8. The average percentage increases in SNS current amplitude in response to forskolin and 8-bromo cAMP were significantly larger than those observed for the mutant SNS(SA). The markedly reduced effects of both forskolin and 8-bromo cAMP were consistent with the major substrates for PKA phosphorylation having been eliminated in SNS(SA) channels.

DISCUSSION

Several pieces of evidence suggest that an increase in voltage-dependent sodium current may underlie the increased excitability of primary afferent neurones after injury (e.g. Devor *et al.* 1993; Waxman *et al.* 1994; Woolf *et al.* 1994). In particular, the TTX-r voltage-dependent sodium channels of sensory neurones are believed to be involved in nociceptive transmission since they are associated predominantly with the nociceptive C fibre neurones (Roy & Narahashi, 1992; Arbuckle & Docherty, 1995; Villière & McLachlan, 1996). Recent evidence also suggests that TTX-r channels in DRGs provide a common target for a number of hyperalgesic agents, e.g. PGE_2, adenosine and serotonin, and that cAMP-dependent PKA phosphorylation of these channels may provide the mechanism for the hyperalgesic responses of these sensory neurones (e.g. Taiwo & Levine, 1991; Ouseph *et al.* 1995; England *et al.* 1996; Gold *et al.* 1996). On this basis, we have investigated PKA phosphorylation of the TTX-r channel α-subunit, SNS, which is selectively expressed in sensory neurones (Akopian *et al.* 1996). Using site-directed mutagenesis we have shown that PKA phosphorylation sites located within the intracellular I–II loop of SNS are the major substrates responsible for PKA modulation of the SNS channel.

Characterization of SNS expressed in COS-7 cells

The functional expression of SNS (PN3) was recently achieved in *Xenopus* oocytes (Akopian *et al.* 1996; Sangameswaran *et al.* 1996), and here we report expression of SNS in a mammalian system. Transient transfection of COS-7 cells with SNS cDNA resulted in the expression of channels producing inward current with qualitatively similar properties to those described previously for native TTX-r channels expressed in cultured sensory neurones (e.g. Roy & Narahashi, 1992; Ogata & Tatebayashi, 1993; Elliott & Elliott, 1993). No endogenous currents were observed in either mock-transfected or non-transfected cells. Na^+ substitution experiments in which external Na^+ was substituted with equimolar choline chloride confirmed that the current observed in SNS-transfected cells was carried by a 'pure' Na^+ conductance. Cd^{2+}, which at 50 μM is sufficient to block endogenous voltage-dependent calcium channels in DRGs whilst leaving the TTX-r sodium current unaffected, was without effect on SNS currents (Tatebayashi & Ogata, 1992; Ogata & Tatebayashi, 1993). Furthermore, the alkaloid veratridine which specifically modifies Na^+ channel gating, induced a 'classic' response in SNS, where large and prolonged tail currents were observed upon repolarization to −90 mV but current amplitude was slightly reduced at depolarized potentials.

Whilst the SNS current possessed similar pharmacological properties to those of native TTX-r current, as outlined above, the voltage dependence of activation for SNS was found to occur at markedly depolarized potentials compared with endogenous currents in DRGs. $V_{½}$ for activation derived from conductance–voltage plots was −2·1 mV for

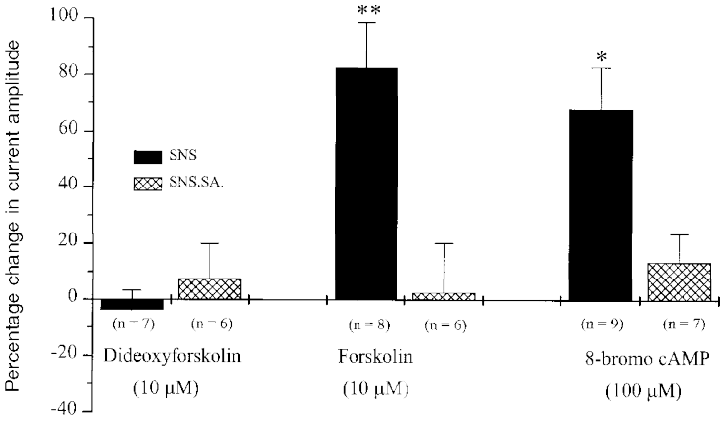

Figure 8. Summary bar-chart showing the effects of dideoxyforskolin (10 μM), forskolin (10 μM) and 8-bromo cAMP (100 μM) on SNS and SNS(SA)

Each bar represents the mean percentage change in current amplitude for SNS (■) and SNS(SA) (▩). Asterisks indicate statistically significant differences between SNS and SNS(SA): * $P < 0{\cdot}05$ and ** $P < 0{\cdot}01$ (Student's unpaired t test).

SNS current in COS-7 cells compared with typically reported values in the range −16 to −10 mV for endogenous TTX-r currents (e.g. Roy & Narahashi, 1992; Elliott & Elliott, 1993; Ogata & Tatebayashi, 1993). A similarly depolarized activation threshold of current was observed when SNS (PN3) was expressed in *Xenopus* oocytes, where currents were reported to peak at between +10 and +20 mV in the presence of 81–115 mM external Na^+ (Akopian *et al.* 1996; Sangameswaran *et al.* 1996). When expressed in COS-7 cells, SNS typically peaked between +10 and +20 mV in the presence of 100 mM $[Na^+]_o$. Nevertheless, the reversal potential, V_{rev}, in SNS-transfected cells was within ±4 mV of the predicted value of 58 mV, showing that the current was carried by Na^+.

SNS current was also found to have a slower rate of inactivation than native TTX-r current. At peak current amplitude (+15 mV), the time constant of inactivation, τ_{inact}, was approximately 2·4-fold slower than for endogenous TTX-r current recorded under similar conditions. At peak current amplitude measured at 20–22 °C, τ_{inact}, as fitted by a single exponential, was 12·1 ms for SNS whereas values of 4·8 and 5·0 ms have been reported for native TTX-r currents recorded at 21–23 °C (Elliott & Elliott, 1993; Ogata & Tatebayashi, 1993). The time constant for activation of SNS current ($\tau_{act} = 0{\cdot}95$ ms), however, was within the range 0·6–2·2 ms, previously reported for TTX-r currents (Elliott & Elliott, 1993; Ogata & Tatebayashi, 1993). The data we report here for SNS expressed in COS-7 cells were very recently confirmed in HEK293T cells (Gladwell *et al.* 1998). When expressed in these cells, SNS channel current peaked at between +10 and +20 mV, with V_{rev} close to the predicted value of 58 mV. The voltage dependence of activation of current in HEK293T cells could be fitted with a Boltzmann function to give $V_{½} = 1$ mV and $k = 8{\cdot}5$ mV, whilst analysis of inactivation gave a value for τ_{inact} at peak amplitude of 12·7 ms.

The existing literature on TTX-r sodium channels describes currents from a variety of DRG preparations, e.g. adult *versus* neonatal and acutely isolated *versus* long-term culture. Electrophysiological and molecular evidence suggests there may be at least two TTX-r channels in small DRG neurones (Scholz *et al.* 1988; Rush *et al.* 1998; Dib-Hajj *et al.* 1998), although England *et al.* (1998) have recently reported that all TTX-r channels in mouse DRGs are encoded by the *sns* gene. Consequently, the reported values for the major functional properties of DRG TTX-r currents can vary considerably (see Rush *et al.* 1998). Nonetheless, it is clear that whether expressed in *Xenopus* oocytes or mammalian cell lines, the SNS channel has a strikingly depolarized current–voltage relationship and slower inactivation kinetics when compared with any endogenous TTX-r currents previously recorded in DRGs. Similar properties were also observed when SNS (PN3) was expressed in *Xenopus* oocytes (Akopian *et al.* 1996; Sangameswaran *et al.* 1996). Such discrepancies in the biophysical properties of SNS and native TTX-r current were suggested by Akopian *et al.* (1996) to be due to the fact that SNS was expressed without the accessory subunit β1 which is normally present in DRGs (Oh *et al.* 1994). The β1-subunit has been shown to increase the rate of inactivation and to cause a hyperpolarizing shift in the current–voltage relationship when coexpressed with the rat brain IIA, skeletal muscle (SkM1) and cardiac rH1 Na^+ channel α-subunits (Patton *et al.* 1994; Isom *et al.* 1995*b*; Chen & Cannon, 1995; Qu *et al.* 1995). However, coexpression of human sodium channel β1 (homologous with DRG sodium β1) failed to accelerate the inactivation kinetics of PN3 expressed in *Xenopus* oocytes (Sangameswaran *et al.* 1996). It is possible that coexpression of SNS with different β-subunits may explain the different TTX-r currents observed in DRGs.

Site-directed mutagenesis of five PKA consensus sites within the I–II loop of SNS inhibits cAMP-dependent phosphorylation

PKA-mediated phosphorylation has been shown biochemically for neuronal (Costa *et al.* 1982; Rossie & Catterall, 1989; Murphy *et al.* 1993), skeletal muscle (Ukomadu *et al.* 1992) and cardiac (Cohen & Levitt, 1993) isoforms of voltage-dependent sodium channels. *In vivo* studies on the α-subunits of the rat brain IIA and human cardiac (hH1) sodium channels have shown that functional modulation by PKA is dependent on the intracellular I–II loop, a region of low sequence homology amongst the sodium channels (Smith & Goldin, 1996; Frohnwieser *et al.* 1997). Within the I–II loops of the rat brain IIA and rat cardiac channel α-subunits there are multiple sites matching PKA consensus sequences (K/RXXS), which have been shown both biochemically and functionally to be directly involved in PKA phosphorylation of these channels (Murphy *et al.* 1993; Murphy *et al.* 1996; Frohnwieser *et al.* 1997; Smith & Goldin, 1996, 1997). In contrast, the skeletal muscle (SkM1) channel which lacks PKA consensus sites within this region, is not modulated by PKA (Frohnwieser *et al.* 1997).

Within the I–II loop of the SNS α-subunit, five 'strong' PKA consensus sequences have also been identified (Fig. 1). By analogy with the other voltage-dependent sodium channels modulated by PKA, these five consensus sites were therefore considered most likely to be involved in the functional modulation of SNS. In order to investigate this possibility, we used a mutant SNS α-subunit, SNS(SA), in which the five PKA sites were removed by site-directed mutagenesis. Mutations were confirmed by DNA sequence analysis. *In vitro* phosphorylation studies on the I–II loops of the wild-type and mutant channels expressed as GST-fusion proteins, GST-SNS and GST-SNS(SA), respectively, confirmed a marked reduction in PKA phosphorylation in the mutant *versus* wild-type channels. The stoichiometry of phosphorylation, measured as moles of phosphate per mole of protein was reduced 5-fold in the mutant compared with wild-type fusion protein. Tryptic peptide mapping revealed that the wild-type GST-SNS protein fragment was phosphorylated by PKA on multiple serine residues. In mutant GST-SNS(SA), on the other hand, eight of the nine

phosphopeptides produced by the wild-type protein were eliminated. This suggested that the five PKA consensus sites eliminated by site-directed mutagenesis were indeed the principal PKA substrates within the I–II loop of SNS. The residual phosphorylation of the mutant tryptic peptide *in vitro* can most probably be explained by phosphorylation of non-consensus serine and/or threonine residues within this protein fragment.

Electrophysiological comparison of SNS and SNS(SA) channels expressed in COS-7 cells suggested that consensus sites within the I–II loop of SNS were the major substrates required for functional modulation by PKA. Activation of PKA by means of the cAMP analogue, dibutyryl cAMP, and the adenylyl cyclase activator, forskolin, has previously been shown by England *et al.* (1996) to increase TTX-r current amplitude in DRGs, with a concurrent hyperpolarizing shift in both voltage dependence of activation and steady-state inactivation. Upregulation of PKA phosphorylation in SNS-transfected COS-7 cells produced similar results to those described above for the native TTX-r current. Thus, a time-dependent increase in current amplitude associated with a hyperpolarizing shift in $V_{½}$ for activation was observed in wild-type SNS-transfected cells in response to forskolin. Dideoxyforskolin, used as a control for non-PKA-related effects, was without effect on SNS. The cAMP analogue 8-bromo cAMP, although apparently less potent than forskolin, nonetheless induced a time-dependent increase in current amplitude which was consistent with phosphorylation by PKA. In contrast, neither forskolin nor 8-bromo cAMP could induce significant upregulation of mutant SNS(SA) current and no shift in the activation threshold was observed. Thus, a marked reduction in the level of cAMP-dependent PKA phosphorylation, consistent with elimination of the I–II loop PKA consensus sites, was found in the mutant channel.

Although the biophysical properties of SNS and SNS(SA) were similar, one notable difference was apparent in the voltage dependence of activation of current. The activation curve for SNS(SA) was shifted by approximately 10 mV in a depolarizing direction compared with wild-type current, whilst the slope and reversal potential remained unaffected. Accordingly, the rate of current inactivation at hyperpolarized potentials between −10 and +15 mV was noticeably slowed. From this, one may predict a similar shift in the voltage dependence of inactivation, as has previously been reported for native TTX-r current in DRGs (England *et al.* 1996). Further data, however, are required to confirm this. On average, current activation kinetics were not significantly affected although in some cells τ_{act} did also appear to be slowed. Since cAMP-dependent phosphorylation has been reported to cause hyperpolarization of the activation threshold of both the native TTX-r (England *et al.* 1996) and SNS channels (reported here), it is possible that the depolarizing shift observed for activation of the mutant channel SNS(SA), may represent the removal of tonic PKA phosphorylation which normally affects wild-type SNS channels under control conditions. However, as forskolin was able to induce a further hyperpolarization of the current–voltage relationship in the wild-type channels it is possible that the effect may be due to partial tonic phosphorylation in a subpopulation of wild-type channels under control conditions. It might also be seen as evidence that multiple PKA phosphorylation sites are involved in cAMP-dependent modulation of SNS channels. On the basis of our data, the possibility of a direct effect of the serine-to-alanine mutations on channel gating cannot be completely ruled out. However, the serine-to-alanine mutation is highly conservative and as such is unlikely to have a major impact on protein structure. A role for tonic phosphorylation of the wild-type SNS channel, at least when expressed in COS-7 cells, therefore seems likely. Whether this is also true for endogenous TTX-r channels in DRGs is unclear. However, Na^+ channels in rat brain neurones have been reported to be extensively phosphorylated under basal conditions, and phosphatases which selectively target specific PKA phosphorylation sites have been identified (Rossie & Catterall, 1989; Li *et al.* 1992; Chen *et al.* 1995).

Conclusions

Three additional putative PKA phosphorylation sites, originally identified in the sequence of PN3 (Sangameswaran *et al.* 1996) can also be found at the N-terminus, the extracellular region IIS3–IIS4, and in the intracellular II–III loop of SNS (see Fig. 1). Whilst the possible involvement of these additional PKA phosphorylation sites cannot be completely dismissed, we nonetheless conclude from our data that the major substrates required for functional modulation of SNS by PKA are located within the I–II loop.

Deletion and site-directed mutagenesis studies in the rat brain IIA and cardiac rH1 channels suggest that of multiple PKA consensus sequences within the I–II loops, phosphorylation at only one or two serine residues may be required for PKA modulation (Murphy *et al.* 1996; Smith & Goldin, 1997). Determination of the precise roles of individual serine residues in the functional modulation of SNS is currently being investigated using individual serine mutants.

We have shown that upregulation of cAMP-dependent PKA phosphorylation reduces the threshold of activation and increases the amplitude of SNS current, whereas removal of tonic PKA phosphorylation, by elimination of the I–II loop PKA consensus sites, increases the threshold of activation and slows current kinetics. These data are consistent with the previously reported responses of native TTX-r sodium channels to activators of cAMP-dependent phosphorylation (England *et al.* 1996). A reduction in threshold and increase in response of nociceptive neurones is believed to underlie the hyperalgesia associated with tissue injury. Therapies designed specifically to block PKA modulation of TTX-r channels in DRGs may therefore provide novel treatments for pain associated with nociceptor sensitization.

Akopian, A. N., Sivilotti, L. & Wood, J. N. (1996). A tetrodotoxin-resistant voltage-gated sodium channel expressed by sensory neurons. *Nature* **379**, 257–362.

Arbuckle, J. B. & Docherty, R. J. (1995). Expression of tetrodotoxin-resistant sodium channels in capsaicin-sensitive dorsal root ganglion neurones of adult rats. *Neuroscience Letters* **185**, 70–73.

Catterall, W. A. (1992). Cellular and molecular biology of voltage-gated sodium channels. *Physiological Reviews* **72** (suppl.), S15–S41.

Chen, C. & Cannon, S. C. (1995). Modulation of Na^+ channel inactivation by the $\beta 1$ subunit: a deletion analysis. *Pflügers Archiv* **431**, 186–195.

Chen, T.-C., Law, B., Kondratyuk, T. & Rossie, S. (1995). Identification of soluble protein phosphatases that dephosphorylate voltage-sensitive sodium channels in rat brain. *Journal of Biological Chemistry* **270**, 7750–7756.

Cohen, S. A. & Levitt, L. K. (1993). Partial characterisation of the rH1 sodium channel protein from rat heart using subtype-specific antibodies. *Circulation Research* **73**, 735–742.

Costa, M. R. C., Casmellie, J. E. & Catterall, W. E. (1982). Selective phosphorylation of the α subunit of the sodium channel by cAMP-dependent protein kinase. *Journal of Biological Chemistry* **257**, 7918–7921.

Devor, M., Govrin, L. R. & Angelides, K. (1993). *Journal of Neuroscience* **13**, 1976–1992.

Dib-Hajj, S. D., Tyrrell, L., Black, J. A. & Waxman, S. G. (1998). NaN, a novel voltage-gated Na channel, is expressed preferentially in peripheral sensory neurons and down-regulated after axotomy. *Proceedings of the National Academy of Sciences of the USA* **95**, 8963–8968.

Elliott, A. A. & Elliott, J. R. (1993). Characterization of TTX-sensitive and TTX-resistant sodium currents in small cells from adult rat dorsal root ganglia. *Journal of Physiology* **463**, 39–56.

England, S., Bevan, S. & Docherty, R. J. (1996). PGE_2 modulates the tetrodotoxin-resistant sodium current in neonatal rat dorsal root ganglion neurones via the cyclic AMP-protein kinase A cascade. *Journal of Physiology* **495**, 429–440.

England, S., Souslova, V., Akopian, A., Okuse, K., Ogata, N. & Wood, J. N. (1998). Voltage-gated sodium channels in *sns* null mutant mice. *Society for Neuroscience Abstracts* **24**, 1821.

Frohnwieser, B., Chen, L-Q., Schreibmayer, W. & Kallen, R. G. (1997). Modulation of human cardiac channel α-subunit by cAMP-dependent protein kinase and the responsible sequence domain. *Journal of Physiology* **498**, 309–318.

Gladwell, Z. M., Trezise, D. J., Plumpton, C., Xie, X. M. & Tate, S. (1998). Expression and functional analysis of recombinant rat sensory neuron-specific Na^+ channels in a mammalian cell line. *Journal of Physiology* **513.P**, 141*P*.

Gold, M. S., Reichling, D. B., Shuster, M. J. & Levine, J. D. (1996). Hyperalgesic agents increase a tetrodotoxin-resistant Na^+ current in nociceptors. *Proceedings of the National Academy of Sciences of the USA* **93**, 1108–1112.

Hamill, O. P., Marty, A., Neher, E., Sakmann, B. & Sigworth, F. J. (1981). Improved patch-clamp techniques for high-resolution current recording from cells and cell-free membrane patches. *Pflügers Archiv* **391**, 85–100.

Hille, B. (1992). *Ionic Currents of Excitable Membranes,* pp. 607. Sinauer Associates Inc., Sunderland, MA, USA.

Isom, L. L., De Jongh, K. S., Patton, D. E., Reber, B. F., Offord, J., Charbonneau, H., Walsh, K., Goldin, A. L. & Catterall. W. A. (1992). Primary structure and functional expression of the beta 1 subunit of the rat brain sodium channel. *Science* **256**, 839–842.

Isom, L. L., Ragsdale, D. S., De Jongh, K. S., Westbroek, R. E., Reber, B. F. X., Scheuer, T. & Catterall, W. A. (1995*a*). Structure and function of the $\beta 2$ subunit of brain sodium channels, a transmembrane glycoprotein with a CAM motif. *Cell* **83**, 433–442.

Isom, L. L., Scheuer, T., Brownstein, A. B., Ragsdale, D. S., Murphy, B. J. & Catterall, W. A. (1995*b*). Functional co-expression of the $\beta 1$ and Type IIA α subunits of sodium channels in a mammalian cell line. *Journal of Biological Chemistry* **270**, 3306–3312.

Kemp, B. E. & Pearson, R. B. (1990). Protein kinase recognition sequence motifs. *Trends in Biochemical Sciences* **15**, 342–346.

Kunkel, T. A. (1985). Rapid and efficient site-specific mutagenesis without phenotypic selection. *Proceedings of the National Academy of Sciences of the USA* **82**, 488–492.

Li, M., West, J. W., Lai, Y., Scheuer, T. & Catterall, W. A. (1992). Functional modulation of brain sodium channels by cAMP-dependent phosphorylation. *Neuron* **8**, 1151–1159.

Li, M., West, J. W., Numann, R., Murphy, B. J., Scheuer, T. & Catterall, W. A. (1993). Convergent regulation of sodium channels by protein kinase C and cAMP-dependent protein kinase. *Science* **261**, 1439–1442.

MacFarland, R. T., Zelus, B. D. & Beavo, J. A. (1991). High concentrations of a cGMP-stimulated phosphodiesterase mediate ANP-induced decreases in cAMP and steroidogenesis in adrenal glomerulosa cells. *Journal of Biological Chemistry* **266**, 136–142.

Moss, S. J., Docherty, C. A. & Huganir, R. L. (1992). Identification of the cAMP-dependent protein kinase and protein kinase C phosphorylation sites within the major intracellular domains of the beta 1, gamma 2S, and gamma 2L subunits of the gamma-amino-butyric acid type A receptor. *Journal of Biological Chemistry* **267**, 14470–14476.

Murphy, B. J., Rogers, J., Perdichizzi, A. P., Colvin, A. A. & Catterall, W. A. (1996). cAMP-dependent phosphorylation of two sites in the α subunit of the cardiac sodium channel. *Journal of Biological Chemistry* **271**, 28837–28843.

Murphy, B. J., Rossie, S., De Jongh, K. S. & Catterall, W. A. (1993). Identification of the sites of selective phosphorylation and dephosphorylation of the rat brain Na^+ channel by cAMP-dependent protein kinase and phosphoprotein phosphatases. *Journal of Biological Chemistry* **268**, 27355–27362.

Ogata, N. & Tatebayashi, H. (1993). Kinetic analysis of two types of Na^+ channels in rat dorsal root ganglia. *Journal of Physiology* **466**, 9–37.

Oh, Y., Sashihara, S. & Waxman, S. G. (1994). *In situ* hybridization localization of the Na^+ channel beta 1 subunit mRNA in rat CNS neurons. *Neuroscience Letters* **176**, 119–122.

Ouseph, A. K., Khasar, S. G. & Levine, J. D. (1995). Multiple second messenger systems act sequentially to mediate rolipram-induced prolongation of prostaglandin E_2-induced mechanical hyperalgesia in the rat. *Neuroscience* **64**, 769–776.

Patton, D. E., Isom, L. L., Catterall, W. A. & Goldin, A. L. (1994). The adult rat brain $\beta 1$ subunit modifies activation and inactivation gating of multiple sodium channel α subunits. *Journal of Biological Chemistry* **269**, 17649–17655.

Qu, Y., Isom, L. L., Westenbroek, R. E., Rogers, J. C., Tanada, T. N., McCormick, K. A., Scheuer, T. & Catterall, W. A. (1995). Modulation of cardiac Na^+ channel expression in *Xenopus* oocytes by $\beta 1$ subunits. *Journal of Biological Chemistry* **270**, 25696–25701.

Rossie, S. & Catterall, W. A. (1989). Phosphorylation of the α subunit of rat brain sodium channels by cAMP-dependent protein kinase at a new site containing Ser686 and Ser687. *Journal of Biological Chemistry* **264**, 14220–14224.

Roy, M. L. & Narahashi, T. (1992). Differential properties of tetrodotoxin-sensitive and tetrodotoxin-resistant sodium channels in rat dorsal root ganglion neurons. *Journal of Neuroscience* **12**, 2104–2111.

Rush, A. M., Brau, M. E., Elliott, A. A. & Elliott, J. R. (1998). Electrophysiological properties of sodium current subtypes in small cells from adult rat dorsal root ganglia. *Journal of Physiology* **511**, 771–789.

Sandberg, M., Butt, E., Nolte, C., Fischer, L., Halbrugge, M., Beltman, J., Jahnsen, T., Genieser, H. G., Jastoff, B. & Walter, U. (1991). Characterization of Sp-5,6-dichloro-1-β-D-ribofuranosyl-benzimidazole-3′,5′-monophosphorothioate (Sp-5,6-DCl-cBiMPS) as a potent and specific activator of cyclic-AMP-dependent protein kinase in cell extracts and intact cells. *Biochemical Journal* **279**, 521–527.

Sangameswaran, L., Delgado, S. G., Fish, L. M., Koch, B. D., Jakeman, L. B., Stewart, G. R., Sze, P., Hunter, J. C., Eglen, R. M. & Herman, R. C. (1996). Structure and function of a novel voltage-gated, tetrodotoxin-resistant sodium channel specific to sensory neurons. *Journal of Biological Chemistry* **271**, 5953–5956.

Scholz, A., Appel, N. & Vogel, W. (1998). Two types of TTX-resistant and one TTX-sensitive Na^+ channel in rat dorsal root ganglion neurons and their blockade by halothane. *European Journal of Neuroscience* **10**, 2547–2556.

Smith, D. B. & Johnson K. S. (1988). Single step purification of polypeptides expressed in *Escherichia coli* as fusions with glutathione S-transferase. *Gene* **67**, 31–40.

Smith, R. D. & Goldin, A. L. (1996). Phosphorylation of brain sodium channels in the I–II linker modulates channel function in *Xenopus* oocytes. *Journal of Neuroscience* **16**, 1965–1974.

Smith, R. D. & Goldin, A. L. (1997). Phosphorylation at a single site in the rat brain sodium channel is necessary and sufficient for current reduction by protein kinase A. *Journal of Neuroscience* **17**, 6086–6093.

Taiwo, Y. O. & Levine, J. D. (1991). Further confirmation of the role of adenylyl cyclase and of cAMP-dependent protein kinase in primary afferent hyperalgesia. *Neuroscience* **44**, 131–135.

Tatebayashi, H. & Ogata, N. (1992). Kinetic analysis of the $GABA_B$-mediated inhibition of the high-threshold Ca^{2+} current in cultured rat sensory neurones. *Journal of Physiology* **447**, 391–407.

Ukomadu, C., Zhou, J. Y., Sigworth, F. J. & Agnew, W. S. (1992). μI Na^+ channels expressed transiently in human embryonic kidney cells: biochemical and biophysical properties. *Neuron* **8**, 663–676.

Villière, V. & McLachlan, E. M. (1996). Electrophysiological properties of neurons in intact rat dorsal root ganglia classified by conduction velocity and action potential duration. *Journal of Neurophysiology* **76**, 1924–1941.

Waxman, S. G., Kocsis, J. D. & Black, J. A. (1994). Type III sodium channel mRNA is expressed in embryonic but not adult spinal sensory neurons, and is re-expressed following axotomy. *Journal of Neurophysiology* **72**, 466–470.

Woolf, C. J., Safieh, G. B., Ma, Q. P., Crilly, P. & Winter, J. (1994). Nerve growth factor contributes to the generation of inflammatory sensory hypersensitivity. *Neuroscience* **62**, 327–331.

Yuckenberg, P. D., Witney, F., Geisselsoder, J. & McClary, J. (1991). Site-directed *in vitro* mutagenesis using uracil-containing DNA and phagemid vectors. In *Directed Mutagenesis: A Practical Approach*, ed. McPherson, M. J., pp. 27–48. Oxford University Press, Oxford.

Acknowledgements

We thank Ms M. Li and Mrs J. Richards for technical assistance and gratefully acknowledge financial support from the Medical Research Council and The Wellcome Trust. We would also like to thank Dr S. England (Pfizer Central Research, Sandwich, Kent) for useful discussions.

Corresponding author

J. N. Wood: Medawar Building, Department of Biology, University College London, London WC1E 6BT, UK.

Email: j.wood@ucl.ac.uk